metals

MDPI

Article

Study on Mechanochemical Activation-Enhanced Hydrochloric Acid Leaching of Rare Earth Elements from Roasted NdFeB Waste

Chenghong Liu [1,2], Tuo Zhao [1,2,*], Chunlei Guo [1,2], Erdou Li [1,2], Yufang Qin [1,2] and Bo Zhang [1,2]

[1] Baotou Rare Earth Research Institute, Baotou 014000, China; hcliu@brire.com (C.L.)
[2] National Key Laboratory of Baiyunobo Rare Earth Resource Researches and Comprehensive Utilization, Baotou 014000, China
* Correspondence: xtyzhaotuo@brire.com

Abstract

NdFeB waste is an important rare earth secondary resource, and the current industrial practice primarily employs a hydrochloric acid preferential dissolution method to recover rare earth elements (REEs). However, approximately 1% of REEs (e.g., cerium oxide, neodymium oxide, praseodymium oxide, and dysprosium oxide) remain in the leaching residue, resulting in low recovery efficiency. This work puts forward mechanochemical leaching (integrating mechanical activation and acid leaching) to replace traditional agitated leaching, which realizes synchronous mechanical activation and acid leaching within a stirred ball mill. A systematic comparison is conducted between these two leaching technologies, and the influences of operational variables on rare earth leaching efficiency are explored. The experimental results reveal that sustained mechanical grinding can pulverize particles down to the submicron level, induce substantial lattice distortion and amorphous transformation, destroy the physical coating of rare earth-bearing phases by iron oxides, and thereby drastically improve the extraction efficiency of REEs. The optimal conditions were determined as follows: stirring speed of 700 r/min, leaching temperature of 85 °C, HCl concentration of 1 mol/L, leaching time of 180 min and solid–liquid ratio of 100 g/L. Furthermore, this study reveals the synchronous evolution mechanism of particle refinement and phase transformation during mechanochemical leaching, providing an alternative and more economical recycling route for NdFeB waste.

Keywords: rare earth elements; mechanical activation; leaching; NdFeB waste

Check for updates

Academic Editor: Srecko Stopic

Received: 16 June 2026
Revised: 12 July 2026
Accepted: 13 July 2026
Published: 11 August 2026

Copyright: © 2026 by the authors. Licensee MDPI, Basel, Switzerland. This article is an open access article distributed under the terms and conditions of the Creative Commons Attribution (CC BY) license.

1. Introduction

Rare earth elements have been extensively applied in high-tech industries owing to their excellent physical and chemical characteristics [1–4]. Currently, approximately 26% of rare earth resources are consumed for manufacturing NdFeB permanent magnets, which have become the highest-output and most broadly adopted rare earth permanent magnet materials [5]. Driven by the accelerated development of strategic emerging sectors including new energy vehicles, wind power generation, energy saving and environmental protection, the downstream application scenarios of NdFeB permanent magnet materials keep expanding, alongside growing market demand for high-grade performance magnets [6,7]. However, during the production of neodymium-iron-boron rare earth permanent magnets and subsequent machining processes, approximately 30% of the material is wasted

as scrap [8]. In addition, once diverse electronic devices reach their end-of-life stage, statistics indicate that more than 10,000 tons of NdFeB waste are produced annually from waste electrical and electronic equipment [9]. This waste contains 20–30% rare earth elements and is rich in valuable metals like iron. In the context of the circular economy, the recovery of valuable metals from waste sources has gained increasing attention, as it not only mitigates environmental pollution but also addresses the continuous depletion of natural resources [10]. The transformation of waste-based materials into high-value-added products represents a promising pathway towards sustainable resource utilization. For NdFeB permanent magnet waste, which contains significant amounts of rare earth elements, developing efficient recovery technologies is crucial for closing the material loop and reducing dependency on primary mining.

In recent years, the recovery of rare earth from NdFeB waste has been widely studied [11]. The recovery methods for rare earth elements are mainly divided into two types: hydrometallurgy and pyrometallurgy approaches [12–17]. The hydrometallurgy approaches include the solvent extraction method, co-precipitation method, selective precipitation method, electroreduction-oxidation method and oxalate precipitation method. These processes have strong adaptability to raw materials, and usually need to consume a lot of acid or alkali for leaching, which is harmful to the environment. The pyrometallurgy approaches include the chlorination pulping method, alloy method, selective oxidation method and calcium reduction method. These processes recover rare earth elements based on changing the chemical state of the elements in the material at high temperatures through oxidation or chlorination reactions. Compared with hydrometallurgical processes, these processes have the disadvantages of small treatment capacity, low recovery, non-selectivity, and high energy consumption. Currently, the hydrochloric acid preferential dissolution method is the most feasible and widely used method in industry [5,18–20], and the process flow is shown in Figure 1. In this process, NdFeB waste is pretreated by crushing and screening, and then oxidized and roasted in a rotary kiln at high temperature to convert metallic rare earth and iron into stable oxides [18]. After roasting, the appropriate temperature and liquid-solid ratio are controlled, and hydrochloric acid is used for selective preferential leaching, so that rare earth oxides are fully dissolved into the liquid phase, and impurities such as iron and aluminum remain in the form of solid slag. Unfortunately, there are about 1% rare earth elements in the NdFeB leaching residues [5]. Therefore, an enhanced leaching method is urgently needed, which has a favorable impact on the leaching of rare earth elements.

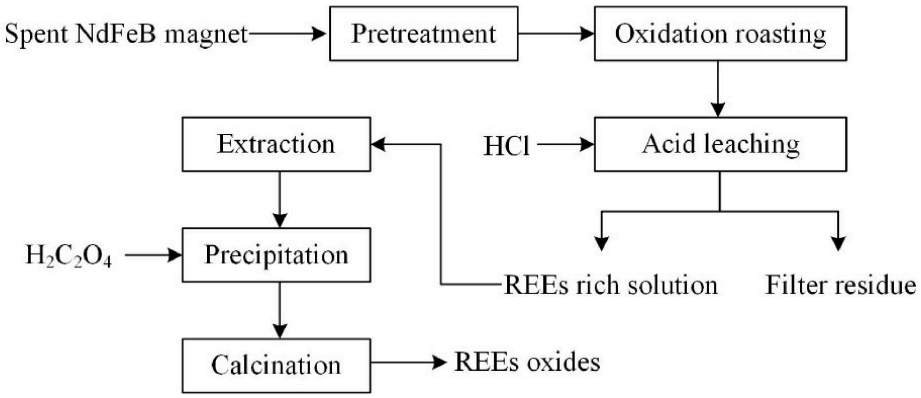


Figure 1. Schematic diagram of hydrochloric acid preferential dissolution method.

Meanwhile, the mechanical activation method as an enhanced leaching method has attracted more and more attention for recycling rare earth second resource [21–26], such as the recycling of scintillation crystal waste, lamp phosphors, REF_3 smelting slag, blast

furnace slag, and other waste containing rare earths. Previous studies have validated mechanical activation coupled with acid leaching as an effective route to extract rare earths from NdFeB scraps [27]. Mechanical activation alters the morphology and reactivity of materials through mechanical force, thereby reducing their dependence on conditions such as reaction temperature and leaching agent concentration [28]. However, these studies employed planetary mills as mechanical activation devices and focused solely on pure magnetic waste materials for waste pretreatment purposes only, without combining them with acid leaching. This mechanical pretreatment primarily enhances leaching in the early stages but does little to improve subsequent dissolution. In other words, the mechanical activation and acid leaching processes are performed separately in time, sequentially in different reactors under varying operational conditions, causing the defects or other metastable forms created in the minerals during mechanical activation to decay before acid leaching [29–31]. Therefore, the use of mechanochemical leaching (simultaneous grinding and leaching) for the recovery of REEs from NdFeB waste was proposed here.

In this work, a one-step process involving mechanical activation and acid leaching is proposed to recover REEs from roasted NdFeB waste. Firstly, the phase composition, particle size and microscopic morphology of the raw material were systematically characterized. Then, the leaching performances of stirring leaching and mechanochemical leaching were compared, and the strengthening mechanism of mechanical force was analyzed by means of XRD, SEM-EDS and particle size detection. Meanwhile, the effects of stirring speed, leaching temperature, HCl concentration and solid–liquid ratio on the leaching efficiency of REEs and Fe were investigated via single-factor experiments to optimize the process parameters. Finally, the evolution rules of mineral phase and particle morphology during mechanochemical leaching were explored, and the stage characteristics and synergistic mechanism of the whole leaching process were revealed.

2. Experimental

2.1. Raw Materials

The samples used in this study are provided by an NdFeB resource recovery company. Various types of neodymium-iron-boron waste (such as NdFeB slurry, NdFeB cutting materials, and NdFeB disassembly materials) were pretreated and then uniformly mixed in a predetermined ratio. The raw materials were charged from the kiln tail for oxidative roasting and then discharged. To ensure full oxidation of both rare earth and iron, the gas (air or slightly oxygen-enriched air) flows in the opposite direction to the raw material. As far as we know, there is little research on recycling rare earth elements from NdFeB oxidized roasting materials. The samples were dried (105 °C, 24 h) and milled to a finer particle size. The main chemical components of the samples were detected by chemical analysis methods, and the results are shown in Table 1. Hydrochloric acid (HCl), consistent with actual industrial production, was used as the leaching agent, purchased from Foshan Xilong Chemical Co., Ltd. (Foshan, China).

Table 1. Chemical composition of raw materials (mass fraction/%).

Elements	Fe	Ce	Pr	Nd	Al	Si	Co	B	Cu
Content (wt%)	42.39	3.77	2.99	9.61	2.44	4.55	0.3	0.56	0.22

2.2. Leaching Experiment

The leaching experiment was conducted in a stirring ball mill with a capacity of 2 L, and the schematic diagram is shown in Figure 2. ZrO_2 balls were used as the grinding media, and the reaction temperature was controlled by circulating water through the jacket.

In each experiment, ZrO_2 balls and the leaching agent were added for preheating, and samples were added for leaching experiments when the predetermined temperature was reached. The different conditions and variable ranges used in the experiment are shown in Table 2. After the reaction, the product was filtered and separated, and the resulting samples were sealed for characterization. The leaching efficiency (%) is defined as:

$$\text{Leaching recovery (\%)} = (C_i \times \text{V})/(\text{M} \times \omega_i) \quad (1)$$

where C_i is the concentration of an element in the leachate (g/L); V is the volume of leachate (L); M is the mass of the solid sample (g); and ω_i is the amount of an element in the solid sample.

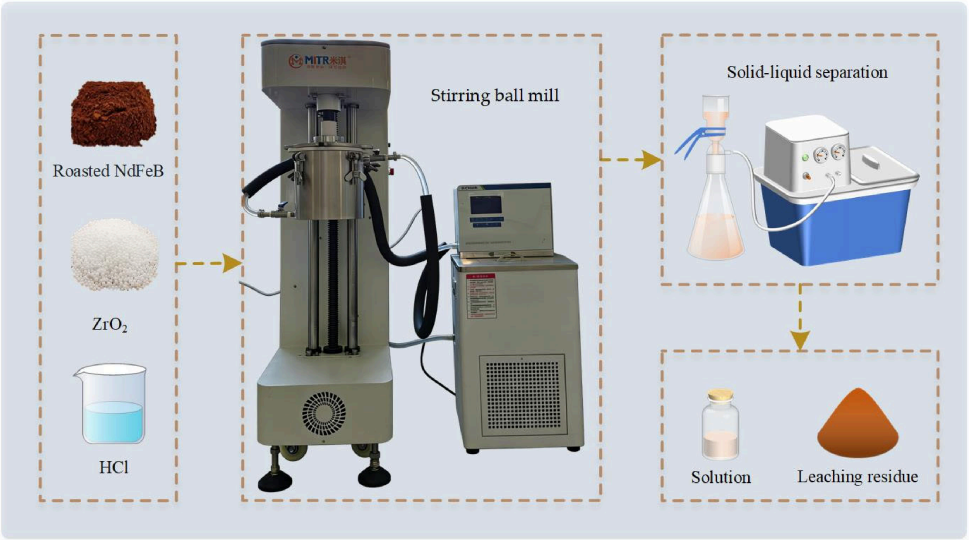


Figure 2. Schematic diagram of stirring ball mill.

Table 2. Different conditions and variable ranges used in the experiment.

Parameters	Values
HCl concentrations, mol/L	0.5, 1.0, 1.5, 2.0, 3.0
Leaching times, min	15, 30, 30, 90, 120, 150, 180
Leaching temperatures, °C	55, 65, 75, 85, 95
Stirring speed, r/min	400, 500, 600, 700, 800
Solid–liquid ratios, g/L	40, 60, 80, 100, 120

The main chemical reactions that occur during the leaching process are as follows:

$$FeO + 2HCl = FeCl_2 + H_2O \quad (2)$$

$$2Fe_2O_3 + 6HCl = 2FeCl_3 + 3H_2O \quad (3)$$

$$2Nd_2O_3 + 6HCl = 2NdCl_3 + 3H_2O \quad (4)$$

$$NdFeO_3 + 6HCl = NdCl_3 + FeCl_3 + 3H_2O \quad (5)$$

2.3. Analytical Methods

The chemical analysis of roasted NdFeB and elements in solution was determined by inductively coupled plasma-optical emission spectroscopy (ICP-OES, 511 VDV, Agilent Technologies, Inc., Santa Clara, CA, USA). The main mineral phases of the samples

were analyzed by X-ray diffraction (XRD, PANalytical X'Pert Pro Powder, Almelo, The Netherlands) with a data collection range of 10–90° at a rate of 5°/min. The morphology of the samples was analyzed by scanning electron microscopy (SEM-EDS, Sigma 500, Zeiss, Oberkochen, Germany) at an accelerating voltage of 20.00 kV. The particle size distributions of the samples were measured by Laser particle size analyzer (MS2000, Malvern Panalytical, Malvern, UK) in liquid mode; the specific surface area was obtained from the particle size distribution.

3. Results and Discussion

3.1. Characterization of Roasted NdFeB

The particle size distribution and XRD pattern of roasted NdFeB are presented in Figure 3. As shown in Figure 3a, the particle size distribution curve exhibits a unimodal normal distribution, with the peak concentrated in the 10–20 μm range. The values of D_{10}, D_{50}, and D_{90} are 2.82 μm, 14.0 μm, and 43.4 μm, respectively. The peak is located around 10 μm, closely matching the median particle size (d_{50}), indicating excellent overall particle size uniformity in the sample without any pronounced bimodal or polycentric distribution patterns. The specific surface area is relatively low, a result directly correlated with particle agglomeration, indicating that NdFeB waste s exhibit significant sintering during the calcination process, with fine primary particles adhering at high temperatures and forming secondary aggregates.

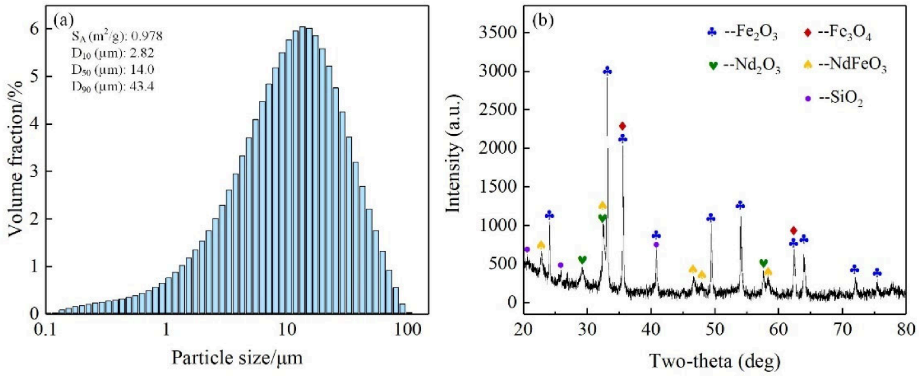


Figure 3. Particle size distribution (**a**) and XRD pattern (**b**) of roasted NdFeB.

As can be seen from the XRD pattern (Figure 3b), the characteristic peaks of the original $Nd_2Fe_{14}B$ phase have completely disappeared, replaced by characteristic peaks of the Fe_2O_3, Fe_3O_4, Nd_2O_3, $NdFeO_3$, and SiO_2 phases. The coexistence of the Fe_2O_3 phase and Fe_3O_4 phase indicates that Fe exists in different oxidation states, reflecting variations in oxygen concentration within the rotary kiln. Areas with low oxygen partial pressure favor the formation of the Fe_3O_4 phase, while areas with high oxygen partial pressure promote the formation of the Fe_2O_3 phase. The valence state of Fe in roasted NdFeB was shown in Table 3. The valence state of Fe in calcined NdFeB is shown in Table 2. The results indicate that MFe accounts for only 2.01%, suggesting that the vast majority of metallic Fe has been oxidized, while a small amount of the $Nd_2Fe_{14}B$ phase that has not been fully oxidized remains encapsulated within the oxide shell. Furthermore, the element neodymium is converted into the Nd_2O_3 and $NdFeO_3$ phases. The Nd_2O_3 phase exhibits high reactivity in acidic leaching systems, whereas the $NdFeO_3$ phase, as a stable perovskite structure, typically requires higher acidity and temperature for effective leaching.

Table 3. Valence state of Fe in roasted NdFeB (mass fraction/%).

Valence State	MFe	Fe^{2+}	Fe^{3+}	Total
Content (%)	0.85	5.41	36.13	42.39
Distribution (%)	2.01	12.76	85.23	100.00

Phase composition and microstructural characterization of roasted NdFeB were investigated, as shown in Figure 4. The sample consists of irregular particles with diameters ranging from 5 to 30 μm, exhibiting well-developed pores and distinct cracks in certain regions, indicating significant volume expansion and phase transformation during calcination. The original dense metallic structure has been replaced by a porous oxide matrix, which facilitates subsequent permeation and mass transfer of the reaction medium during acid leaching. The ESD element mapping results demonstrate that the Fe element exhibits extensive continuous distribution, forming a matrix phase dominated by Fe_2O_3 and Fe_3O_4 phases. The distribution of O element closely matches that of metallic elements such as Fe, Nd, and other metal elements, confirming that the calcination process achieved complete oxidation of the metallic elements, with no significant residual unoxidized metallic phases. Nd element is enriched within the particle interior or at its boundaries, with certain regions overlapping those containing the Fe element, indicating the presence of the $NdFeO_3$ phase, which is consistent with the analysis results of the XRD pattern.

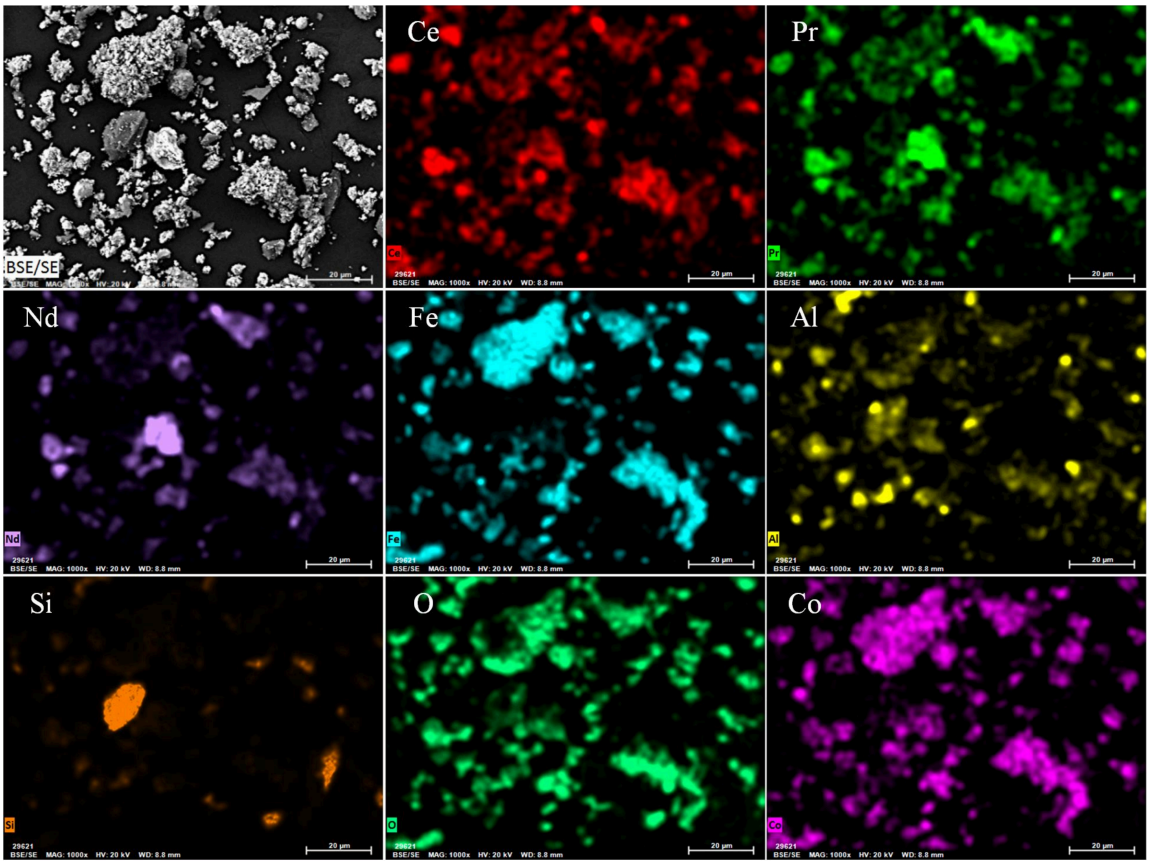


Figure 4. SEM-EDS elemental mapping of roasted NdFeB.

3.2. Comparison of Acid Leaching Methods

A comparative study was conducted on the effects of mechano-chemical leaching and stirring leaching on the leaching efficiency of REEs and Fe at different times, as shown in Figure 5. These experiments were carried out under the following conditions: reaction

temperature of 85 °C, HCl concentration of 1.0 mol/L, stirring speed of 700 r/min, and solid–liquid ratio of 100 g/L. The results indicated that the leaching efficiency of REEs and Fe increased with increasing leaching time for both methods, exhibiting a typical pattern of "rapid rise--slow growth--stabilization". However, mechanical activation has significant differences in its strengthening effects on Fe and REEs.

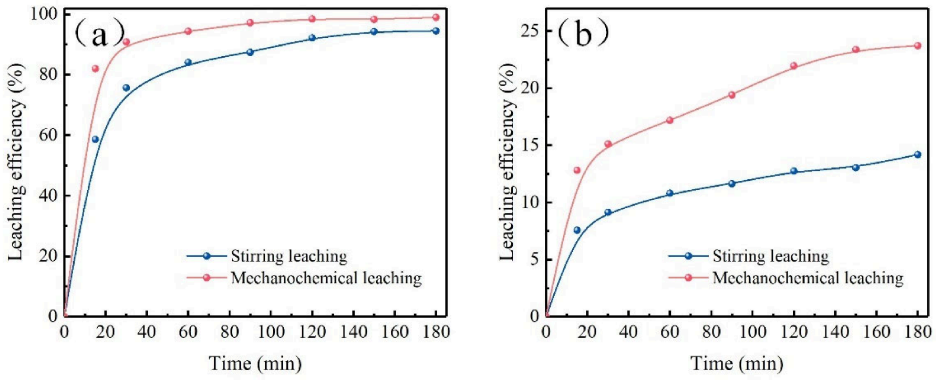


Figure 5. Effect of reaction time on leaching efficiency: (**a**) REEs (**b**) Fe.

The leaching efficiency of REEs rose rapidly in the first 15 min, and the leaching efficiency of REEs in the stirring leaching method was 58.59%, while the leaching efficiency of REEs in the mechano-chemical leaching method was 82.04%. This indicates that mechanical activation significantly accelerated the process of hydrochloric acid leaching. When the leaching time was extended to 30 min, the leaching efficiency of REEs in the mechano-chemical leaching method was 90.84%. As the leaching time was further extended, the leaching efficiency of REEs increased gradually and stabilized at 120 min.

The leaching behavior of Fe is obviously different from that of REEs, and mechanical activation has a more significant effect on the leaching efficiency of Fe. The final leaching efficiency of Fe is increased from 14.18% to 23.72%, while that of REEs is increased by about 5%. This is mainly due to the difference in mineral occurrence state between Fe and REEs. Fe element predominantly exists as an iron oxide phase in NdFeB waste residue. Although mechanical activation enhances the leaching efficiency of Fe, the absolute improvement is limited, which shows that the poor leachability of Fe comes from physical wrapping and is more affected by its chemical stability. In contrast, REEs mainly exist in the NdFeB waste residue as an easily leachable rare earth oxide phase, which has high reactivity in the stirring leaching process. While mechanical activation offers limited improvement in REEs extraction efficiency, it significantly reduces the reaction time.

The XRD patterns of leaching residue with different leaching methods were shown in Figure 6. Due to the low REEs content in the leach residues, no distinct diffraction peaks from REEs phases were observed. The main phases in both leaching residues are Fe_2O_3, Fe_3O_4, and SiO_2 phases. Furthermore, the characteristic peaks of the residues from the stirring leaching process are sharp and intense, indicating well-developed crystallinity in the residues. In contrast, the intensities of the diffraction peaks for all phases in the residues from the mechano-chemical leaching process are significantly reduced, with the peak shapes broadening and becoming flatter. This phenomenon can be attributed to two main factors: first, mechanical grinding causes severe lattice distortion and amorphization in the mineral particles, reducing crystal order and leading to decreased diffraction peak intensity and broadening of the peaks; second, mechanical forces promote the decomposition and dissolution of iron oxides, causing more Fe element to dissolve into the solution and reducing the absolute content of Fe element in the leaching residue.

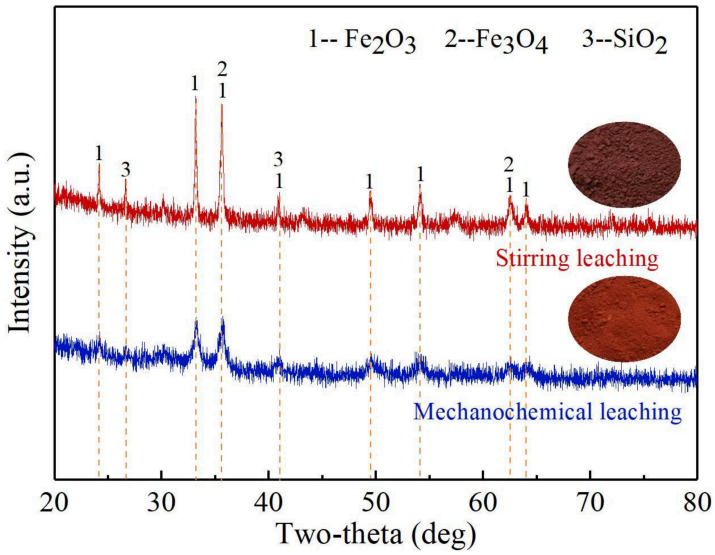


Figure 6. XRD pattern of leaching residue with different leaching methods.

The SEM images of leaching residue with different leaching methods were shown in Figure 7a,b. For the residue with stirring leaching (Figure 7a), the particles are irregular in shape, the overall structure of the particles remains relatively intact, while their surfaces are covered with erosion pits and cracks. For the residue with mechano-chemical leaching (Figure 7b), the particle size is significantly finer, with no obvious large agglomerates between particles, and the particle surfaces are porous with a uniform size distribution. The particle size distribution data in Figure 8 further quantify these differences. For the residue with mechano-chemical leaching, the values of D_{50}, D_{90}, and D_{100} are 0.88 μm, 2.43 μm, and 18.6 μm, respectively, indicating that the particles have been thoroughly crushed to a fine scale with a relatively concentrated distribution. In contrast, the particle size of stirring leaching residues is significantly coarser, and the values of D_{50}, D_{90}, and D_{100} are 11.2 μm, 36.4 μm, and 97.9 μm, respectively, indicating a broader particle size distribution with a higher proportion of coarse particles. This difference is highly consistent with the SEM morphology. Furthermore, these differences in morphological characteristics reflect the distinct effects of different processing methods on particles: the stirring leaching method merely achieves solid–liquid mixing without promoting particle dissociation, whereas the mechanical activation leaching method effectively refines particles and disrupts their original structure.

To further investigate the distribution patterns of unexposed REEs in the leaching residue from the stirring leaching method, the SEM-EDS analysis results of the leaching residue are shown in Figure 7c. The distributions of Fe and O elements largely overlap, with iron oxides forming the basic framework. REEs exhibit a distinctly non-uniform distribution, and their distribution range is significantly smaller than that of the Fe element; they are spatially enclosed by the iron oxide phase. This indicates that residual rare earth elements are primarily embedded within iron oxide particles rather than existing as independent mineral phases, which is also a key reason for the low leaching efficiency in the stirring leaching process. In contrast, mechanical activation continuously applies mechanical force to disrupt the particle structure, breaking the encapsulation of the REEs phases by the iron oxide phase and promoting the full exposure of the REEs phases, thereby facilitating their participation in the acid leaching reaction and achieving a higher leaching efficiency.

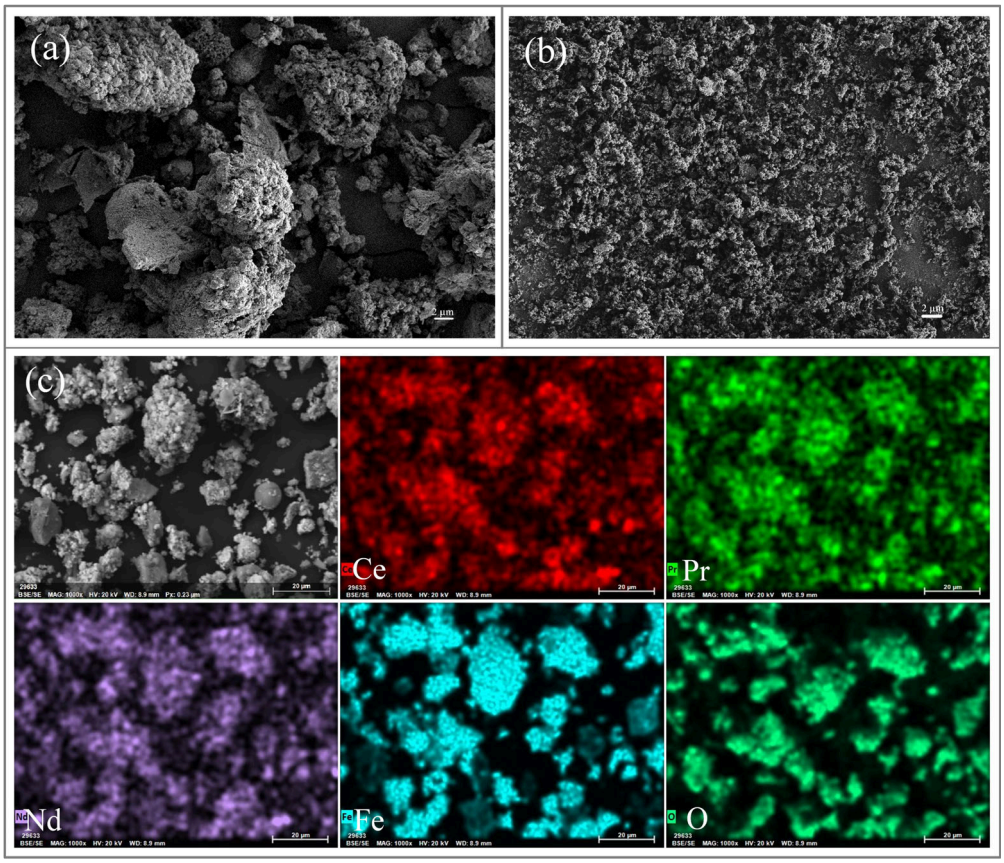


Figure 7. SEM image of leaching residue with stirring leaching (**a**) and mechano-chemical leaching (**b**,**c**); SEM-EDS elemental mapping of residue with stirring leaching.

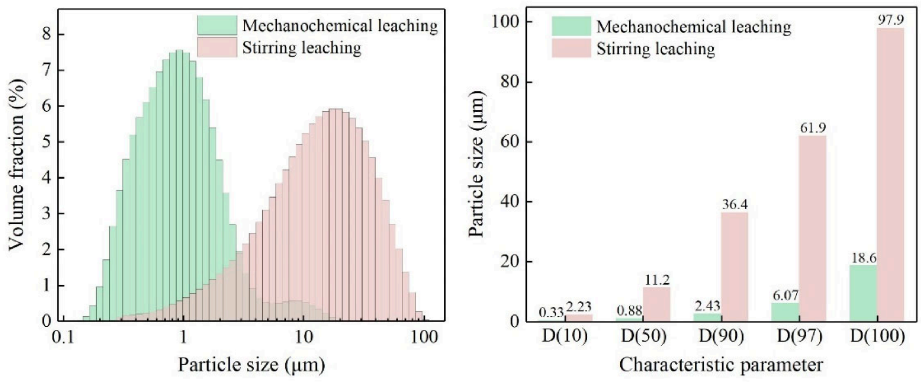


Figure 8. Particle size distribution of leaching residue with different leaching methods.

3.3. Effect of Operating Parameters on Leaching Process

To optimize the mechanochemical leaching process, the effects of operating parameters (leaching temperature, HCl concentration, liquid-solid ratio, and stirring speed) on the leaching efficiency of REEs and Fe were investigated.

The effect of stirring speed on the leaching efficiency of REEs and Fe was carried out in the range of 400–800 r/min in 1 mol/L HCl solution at a temperature of 85 °C with a solid–liquid ratio of 100 g/L for 180 min leaching time, as shown in Figure 9a. The results show that both the leaching efficiencies of REEs and Fe increase with increasing stirring speed. Due to excessively low stirring speeds potentially causing particle sedimentation, the leaching efficiency of REEs was only 79.17% at a stirring speed of 400 r/min. When the stirring speed reached 700 r/min, the leaching efficiency of REEs was 99.03%. Further

increasing the speed to 800 r/min did not significantly affect the leaching efficiency, indicating that the leaching of REEs had approached reaction equilibrium at around 700 r/min. Considering that excessively high stirring speed increases energy consumption and equipment wear while having a negligible effect on leaching efficiency, 700 r/min is selected as the optimal stirring speed.

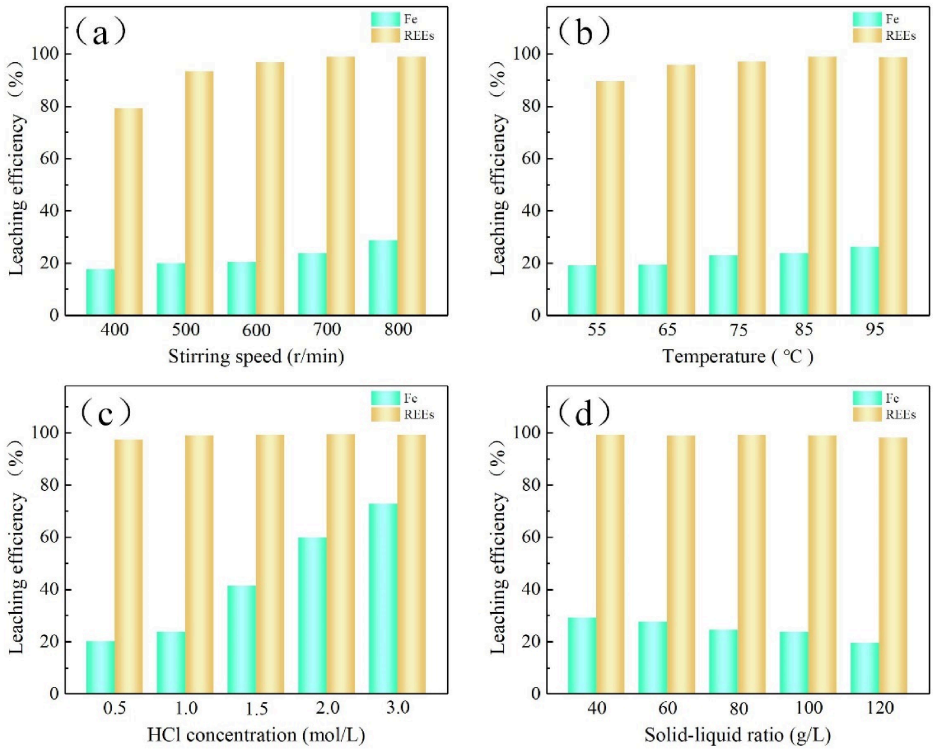


Figure 9. Effect of operating parameters on leaching process: (**a**) stirring speed, (**b**) leaching temperature, (**c**) HCl concentration, (**d**) liquid-solid ratio.

The effect of temperature on the leaching efficiency of REEs and Fe was carried out in the range of 55–95 °C in 1 mol/L HCl solution at a stirring speed of 700 r/min with a solid–liquid ratio of 100 g/L for 180 min leaching time, as shown in Figure 9b. The results showed that temperature has a positive effect on the leaching efficiency of REEs and Fe, but there were significant differences between them. The leaching efficiency of REEs reached about 89.54% at 55 °C, and it was close to equilibrium at 85 °C. Further heating to 95 °C did not result in any significant change in leaching efficiency. The leaching efficiency of Fe increased continuously with the increase in temperature, and there was no plateau period, which indicated that the increase in temperature had a continuous promoting effect on Fe leaching. Considering that excessively high temperatures increase energy consumption, 85 °C is the ideal leaching temperature.

The effect of HCl concentration on the leaching efficiency of REEs and Fe was carried out in the range of 0.5–3 mol/L at a temperature of 85 °C with a solid–liquid ratio of 100 g/L for a 180 min leaching time, as shown in Figure 9c. The results show that HCl concentration enhances the leaching efficiency of both elements, with the leaching efficiency of Fe being more sensitive to variations in HCl concentration. The leaching efficiency of REEs showed minimal dependence on HCl concentration, indicating that mechanochemical enhancement alone is sufficient to achieve high-efficiency leaching under low acid conditions. In contrast, the leaching efficiency of Fe increased significantly with rising HCl concentration. Especially when the HCl concentration was 3 mol/L, the leaching efficiency of Fe reached as high as 72.76%, making it impossible to achieve selective leaching of rare

earth elements. Considering the subsequent removal of Fe at low acidity, 1 mol/L muriatic acid was chosen.

The effect of solid–liquid ratio on the leaching efficiency of REEs and Fe was carried out in the range of 40–120 g/L in 1 mol/L HCl solution at a temperature of 85 °C with a stirring speed of 700 r/min for 180 min leaching time, as shown in Figure 9d. The solid–liquid ratio primarily influences the leaching process by affecting the effective acid concentration in the leaching system, mass transfer conditions, and the diffusion behavior of ions in the solution. As the solid–liquid ratio increases to 120 g/L, the leaching efficiency of REEs decreases slightly. Thus, 100 g/L was selected as the optimal solid-to-liquid ratio.

3.4. Evolution of Phase and Morphology

The XRD patterns of leaching residues at different times are shown in Figure 10. The characteristic diffraction peaks of the initial sample are sharp and intense, indicating good crystalline integrity, which was consistent with the SEM morphology of roasted NdFeB (Figure 4). The relative intensity of the diffraction peaks decreased as the leaching reaction progressed, while the linewidths of the peaks showed the opposite trend. This is a typical characteristic of mechanically activated products, resulting from grain refinement and lattice distortion caused by the impact and collision of grinding balls. The diffraction peaks of Nd_2O_3 and $NdFeO_3$ phases exhibited a significant intensity decline during the initial leaching stage (15–30 min), and completely disappeared by 60 min. When the leaching time was extended to 180 min, the diffraction peak intensities of Fe_2O_3 and Fe_3O_4 phases continued to weaken progressively, indicating sustained dissolution of iron oxides under prolonged combined mechanical activation and acid leaching. On the whole, mechanical activation preferentially disrupts the crystal structure of rare earth oxides, and the leaching rate of rare earth oxides is significantly higher than that of iron oxides. This indicates that the Fe_2O_3 phase exhibits good resistance to dissolution in the hydrochloric acid system. This difference in phase stability serves as the chemical basis for the preliminary separation of rare earth elements from iron during hydrochloric acid leaching.

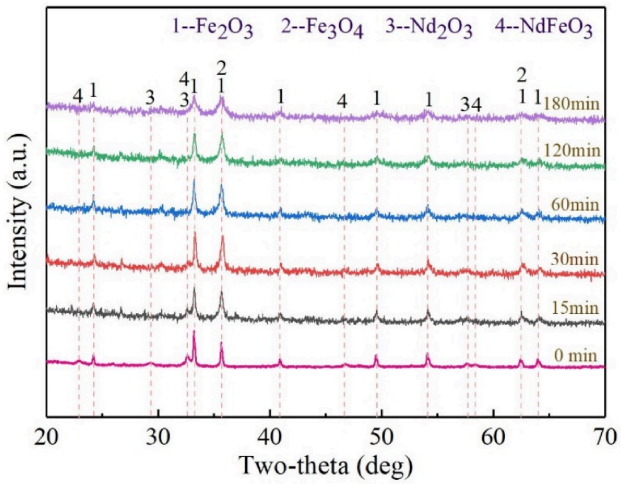


Figure 10. XRD pattern distribution of roasted NdFeB with different roasting times.

The particle size distribution and SEM images of leaching residues at different times were shown in Figures 11 and 12, respectively. Initially, the sample consisted mainly of irregular aggregates with a broad particle size distribution, exhibiting a rough surface yet overall density. At 15 min, the edges of the particles had become significantly blunted, and the large chunks of sample were clearly fragmented into fine powders, with D_{50} decreasing to 3.94 μm, while the surfaces developed fine cracks and erosion pits due to initial acid

corrosion. By 30 min, the particle size further decreased, with D50 decreasing to 2.05 μm, and the original lumpy particles had been broken down into smaller agglomerates. By 60 min, the particles further refined into fine fragmented morphology, with D_{50} and D_{90} values decreasing to 1.85 μm and 4.71 μm, respectively, demonstrating more uniform distribution. When extended to 180 min, the particle morphology remains largely stable, maintaining a fine and uniform floccular structure. The particle size distribution curves further narrowed and converged, with D_{10}, D_{50}, and D_{90} stabilizing at 0.339 μm, 0.862 μm, and 2.55 μm, respectively.

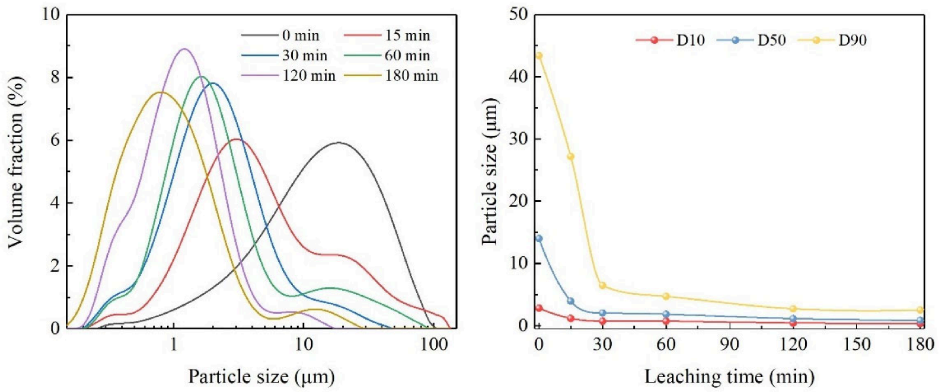


Figure 11. Particle size distribution of roasted NdFeB with different times.

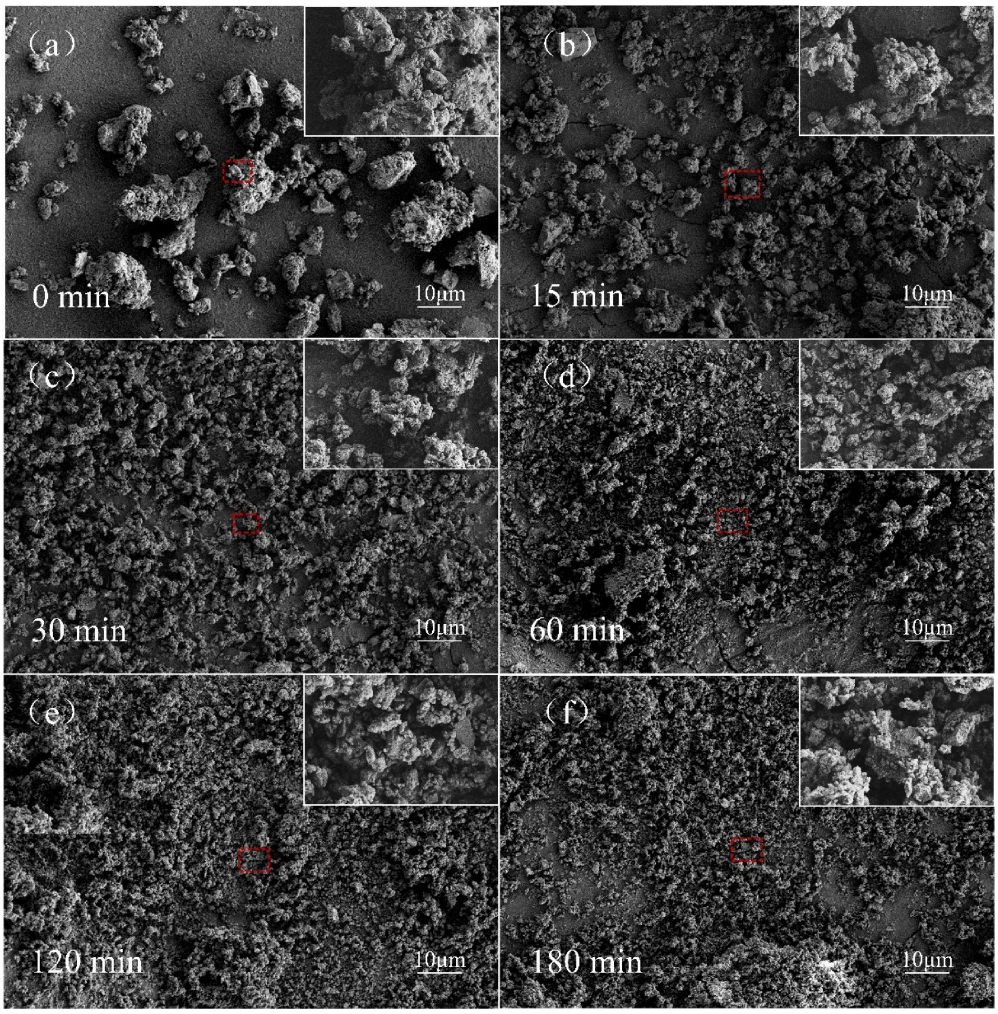


Figure 12. SEM images of roasted NdFeB with different times. (**a**) 0 min; (**b**) 15 min; (**c**) 30 min; (**d**) 60 min; (**e**) 120 min; (**f**) 180 min.

In summary, it is evident that the particle refinement process and the phase transformation process exhibit clear synchrony. During the early leaching stage (0–30 min), mechanical crushing and refinement play a dominant role. The external structure of the particles is directly shattered by the continuous impact and shear forces of mechanical grinding, exposing the encapsulated rare earth phases. This leads to the rapid and preferential dissolution of the REE phases, a phenomenon primarily manifested as the "exposure effect" caused by mechanical activation. During the middle stage of leaching (30–120 min), the particles transition from an aggregated state to a flocculent morphology, with the change in particle size becoming gradual. Mechanical forces reduce the reaction activation energy of phases through crystal chemical effects such as lattice distortion and dislocations, thereby further promoting the continuous progression of leaching reactions. This phenomenon is primarily manifested as the "chemical activation effect" induced by mechanical activation. In the late leaching stage (120–180 min), both particle size and microstructure tend to stabilize. The leaching of REEs is essentially complete, while the phase structure of iron oxides continues to be disrupted by mechanical friction and acid corrosion, leading to a gradual weakening of the diffraction peaks associated with iron oxide phases. The leaching efficiency of Fe rises slowly during this stage, gradually transitioning toward a steady state.

3.5. Comparison of Recycling Methods

Table 4 presents a comparison between the mechanochemical leaching method developed in this work and several similar methods reported in the literature for REEs recovery from NdFeB waste/magnets. It can be seen that most existing studies employ a two-step approach, where mechanical activation is performed first as a pretreatment followed by acid leaching in a separate reactor. This process requires additional energy inputs for material transfer and heating. The mechanically induced defects and metastable phases tend to partially recover before the subsequent leaching step, limiting the overall enhancement effect. In contrast, the present study proposes a one-step mechanochemical leaching process that integrates mechanical activation and acid leaching simultaneously in a stirring ball mill, t significantly reducing energy consumption while achieving a rare earth recovery rate of 99.03% within 180 min.

Table 4. Comparison of different methods for recovering rare earths from NdFeB waste.

Source of Metals Recovered	Solvents	Process	Recovery Efficiency	References
Nickel-coated magnet	$Fe_2(SO_4)_3$	Magnet powder was mixed with $Fe_2(SO_4)_3$ and milled, followed by leaching with water.	>95%	(Loy S V, et al. [26])
Discarded NdFeB magnets	HCl	Mechanical activation followed by acid leaching	99%	(Mao F, et al. [29])
NdFeB cutting material	HCl	Mechanical activation followed by acid leaching	96.1%	(Zhi Z, et al. [2])
Roasted NdFeB waste	HCl	Mechanochemical leaching (simultaneous grinding and leaching)	99%	This study

Moreover, this method exhibits distinct advantages in terms of industrial applicability. Unlike studies that use pristine NdFeB magnets as feedstock, this work specifically targets industrially roasted NdFeB waste. The proposed mechanochemical leaching process can directly replace the conventional stirring leaching step in existing hydrochloric acid preferential dissolution production lines with minimal equipment modification (only requiring stirring ball mills instead of conventional reactors). Although the mechanical grinding

during the process increases electricity consumption compared to conventional stirring leaching, this additional energy input is partially offset by the reduced leaching time and lower acid consumption enabled by the enhanced kinetics. Overall, the proposed method provides an environmentally benign and energy-efficient pathway for sustainable rare earth recovery from secondary resources.

4. Conclusions

This paper investigates the feasibility and mechanism of rare earth recovery from roasted NdFeB waste oxide using the mechanochemical leaching method, and concludes with the following conclusions:

(1) Rare earth elements primarily exist in the forms of Nd_2O_3 and $NdFeO_3$, where their structural inertness combined with the encapsulation effect constitutes the primary obstacle to rare earth leaching.

(2) Compared with stirring leaching, mechanochemical leaching achieves thorough particle comminution, induces lattice distortion and amorphization of minerals, disrupts the encapsulating structure of iron oxides around REE phases, and ultimately increases the final leaching efficiency of REEs by approximately 5%.

(3) Through single-factor experiments, the optimal leaching conditions were determined as follows: HCl concentration of 1.0 mol/L, leaching temperature of 85 °C, stirring speed of 700 r/min, and solid–liquid ratio of 100 g/L. Under these conditions, the leaching efficiency of REEs reached 99.03%, while significantly suppressing the dissolution of iron.

(4) Particle refinement and phase transformation exhibit a clear synchrony during the leaching process. In the early stage (0–30 min), mechanical fragmentation dominates, enabling the rapid and preferential dissolution of rare earth elements by breaking the physical encapsulation of rare earth elements by iron oxides; In the middle stage (30–120 min), chemical activation plays the primary role, with mechanical forces inducing lattice distortions and dislocations, thereby reducing the activation energy of the reaction; in the late stage (120–180 min), the phase structure of the iron oxides continues to be disrupted under the synergistic action of mechanical friction and acid corrosion, and the system approaches a steady state.

(5) Iron in the leachate is separated from REEs by oxidation of Fe^{2+} to Fe^{3+} followed by pH adjustment to 4.0–4.5, at which Fe^{3+} precipitates quantitatively as $Fe(OH)_3$ and is removed by filtration, while REEs remain in solution. This purification step removes over 99.5% of the dissolved iron, providing a qualified solution for subsequent solvent extraction and oxalic acid precipitation.

Author Contributions: Conceptualization, C.L. and T.Z.; methodology, C.L. and B.Z.; software, E.L. and Y.Q.; validation, B.Z.; formal analysis, C.G. and Y.Q.; investigation, C.G. and E.L.; resources, C.G. and E.L.; data curation, C.G. and B.Z.; writing—original draft preparation, C.L. and Y.Q.; writing—review and editing, C.L. and E.L.; visualization, C.G. and E.L.; supervision, T.Z.; project administration, T.Z.; funding acquisition, T.Z. All authors have read and agreed to the published version of the manuscript.

Funding: This research was funded by the Projects of the Northern Rare Earth Group (BFXT-2024-D-0008), and the authors acknowledge the assistance.

Data Availability Statement: Data are contained within the article.

Conflicts of Interest: The authors were employed by the company Baotou Research Institute of Rare Earths, Baotou, China; State Key Laboratory of Baiyunobo Rare Earth Resource Researches and Comprehensive Utilization, Bayan Obo, China. The authors declare that the research was conducted

in the absence of any commercial or financial relationships that could be construed as a potential conflict of interest.

References

1. Zhang, Y.; Gu, F.; Su, Z.; Liu, S.; Anderson, C.; Jiang, T. Hydrometallurgical Recovery of Rare Earth Elements from NdFeB Permanent Magnet Scrap: A Review. *Metals* **2020**, *10*, 841. [CrossRef]
2. Zhihan, Z.; Zhi, W.; Dong, W.; Yong, L.; Wanhai, X.; Chenghao, L.; Yang, L.; Jian, W.; Guobiao, L. A green process for selective REEs recovery from Rare Earth Waste through mechanochemical activation. *Sep. Purif. Technol.* **2023**, *315*, 123654. [CrossRef]
3. Kaya, E.E.; Kaya, O.; Stopic, S.; Gürmen, S.; Friedrich, B. NdFeB Magnets Recycling Process: An Alternative Method to Produce Mixed Rare Earth Oxide from Scrap NdFeB Magnets. *Metals* **2021**, *11*, 716. [CrossRef]
4. Swain, N.; Mishra, S. A review on the recovery and separation of rare earths and transition metals from secondary resources. *J. Clean. Prod.* **2019**, *220*, 884–898. [CrossRef]
5. Kumari, A.; Sinha, M.K.; Pramanik, S.; Sahu, S.K. Recovery of rare earths from spent NdFeB magnets of wind turbine: Leaching and kinetic aspects. *Waste Manag.* **2018**, *75*, 486–498. [CrossRef] [PubMed]
6. Li, C.; Sun, A.; Tian, Z.; Zhang, X.; Ma, B. Efficient reuse of the waste sintered NdFeB magnet with Dy_2O_3 addition. *J. Magn. Magn. Mater.* **2018**, *462*, 41–45. [CrossRef]
7. Xu, Q.; Yang, L.; Wang, D.; Hou, X.; Sun, Y.; Zhou, X.; Zhou, X.; Li, Y. Evaluating the fractionation of ion-adsorption rare earths for in-situ leaching and metallogenic mechanism. *J. Rare Earths* **2018**, *36*, 1333–1341. [CrossRef]
8. Lai, W.; Liu, M.; Li, C.; Suo, H.; Yue, M. Recovery of a composite powder from NdFeB slurry by co-precipitation. *Hydrometallurgy* **2014**, *150*, 27–33. [CrossRef]
9. Hua, Z.; Wang, J.; Wang, L. Selective Extraction of Rare Earth Elements from NdFeB Scrap by Molten Chlorides. *ACS Sustain. Chem. Eng.* **2014**, *2*, 2536–2543. [CrossRef]
10. Abidli, A.; Huang, Y.; Rejeb, Z.B.; Zaoui, A.; Park, C.B. Sustainable and efficient technologies for removal and recovery of toxic and valuable metals from wastewater: Recent progress, challenges, and future perspectives. *Chemosphere* **2022**, *292*, 133102. [CrossRef] [PubMed]
11. Jha, M.K.; Kumari, A.; Panda, R.; Kumar, J.R.; Yoo, K.; Lee, J.Y. Review on hydrometallurgical recovery of rare earth metals. *Hydrometallurgy* **2016**, *165*, 2–26. [CrossRef]
12. He, L.; Xu, Q.; Li, W.; Dong, Q.; Sun, W. One-step separation and recovery of rare earth and iron from NdFeB slurry via phosphoric acid leaching. *J. Rare Earths* **2022**, *40*, 338–344. [CrossRef]
13. Uda, T. Recovery of Rare Earths from Magnet Sludge by $FeCl_2$. *Mater. Trans.* **2002**, *44*, 55–62. [CrossRef]
14. Takeda, O.; Okabe, T.H.; Umetsu, Y. Phase equilibrium of the system Ag–Fe–Nd, and Nd extraction from magnet scraps using molten silver. *J. Alloys Compd.* **2004**, *379*, 305–313. [CrossRef]
15. Nakamoto, M.; Kubo, K.; Katayama, Y.; Tanaka, T.; Yamamoto, T. Extraction of rare earth elements as oxides from a neodymium magnetic sludge. *Metall. Mater. Trans. B* **2012**, *43*, 468–476. [CrossRef]
16. Tian, Y.L.; Liu, Z.W.; Zhang, G.Q. Recovering REEs from NdFeB wastes with high purity and efficiency by leaching and selective precipitation process with modified agents. *J. Rare Earths* **2019**, *27*, 205–210. [CrossRef]
17. Itakura, T.; Sasai, R.; Itoh, H. Resource Recovery from NdFeB Sintered Magnet by Hydrothermal Treatment. *J. Alloys Compd.* **2006**, *408*, 1382–1386. [CrossRef]
18. Hoogerstraete, T.V.; Blanpain, B.; Gerven, T.V. From NdFeB magnets towards the rare-earth oxides: A recycling process consuming only oxalic acid. *RSC Adv.* **2014**, *4*, 64099–64111. [CrossRef]
19. Liu, F.; Porvali, A.; Wang, J.; Wang, H.; Peng, C.; Wilson, B.P.; Lundström, M. Recovery and separation of rare earths and boron from spent Nd-Fe-B magnets. *Miner. Eng.* **2019**, *145*, 106097.
20. Lee, J.C.; Kim, W.B.; Jeong, J.; Yoon, I.J. Extraction of neodymium from Nd-Fe-B magnet scraps by sulfuric acid. *J. Kor. Inst. Met. Mater.* **1998**, *36*, 967–972.
21. Chen, H.; Liu, Y.; Zhou, X.; Zhang, W.; Ju, P.; Zhong, X.; Lin, J.; Wan, Y.; Li, X. Moderate strategy for efficient recovery of rare earth elements from scintillation crystal waste. *Chem. Eng. J.* **2024**, *500*, 156815. [CrossRef]
22. Song, G.; Yuan, W.; Zhu, X.; Wang, X.; Zhang, C.; Li, J.; Bai, J.; Wang, J. Improvement in rare earth element recovery from waste trichromatic phosphors by mechanical activation. *J. Clean. Prod.* **2017**, *151*, 361–370. [CrossRef]
23. Liu, Y.; Gao, F.; Chen, T.; Wang, C.; Hu, K.; Zhang, C.; Huang, Z.; Li, X.; Wan, Y. Effective recovery of rare earth and fluorine from REF_3 smelting slag by a mechanochemical process. *Sep. Purif. Technol.* **2023**, *316*, 123832. [CrossRef]
24. Loy, S.V.; Nal, M.A.R.; Binnemans, K.; Van Gerven, T. Recovery of valuable metals from NdFeB magnets by mechanochemically assisted ferric sulfate leaching. *Hydrometallurgy* **2020**, *191*, 105154. [CrossRef]
25. Sim, G.; Park, Y.; Hong, S.; Seo, D.; Moon, S.; Cho, J.; Park, Y. Alkali fusion-enhanced metal leaching of blast furnace slag for pretreatment of simultaneous carbon mineralization and rare earth elements recovery. *Chem. Eng. J.* **2025**, *505*, 159762. [CrossRef]

26. Shukla, N.; Dhawan, N. Comparison of processing routes for recovery of rare earth elements from discarded fluorescent lamp phosphors. *Miner. Eng.* **2022**, *187*, 107759. [CrossRef]
27. Mao, F.; Zhu, N.; Zhu, W.; Liu, B.; Wu, P.; Dang, Z. Efficient recovery of rare earth elements from discarded NdFeB magnets by mechanical activation coupled with acid leaching. *Environ. Sci. Pollut. Res.* **2022**, *29*, 25532–25543. [CrossRef]
28. Yu, Y.S.; Cui, L.X.; Zhang, L.B.; Wang, Y.F. Efficient mechanochemical leaching of zinc from zinc oxide ores. *Trans. Nonferrous Met. Soc. China* **2024**, *34*, 1976–1993. [CrossRef]
29. Tiechui, Y.; Qinyuan, C.; Jie, L. Effects of mechanical activation on physicochemical properties and alkaline leaching of hemimorphite. *Hydrometallurgy* **2010**, *104*, 136–141. [CrossRef]
30. Li, C.; Liang, B.; Chen, S.P. Combined milling–dissolution of Panzhihua ilmenite in sulfuric acid. *Hydrometallurgy* **2006**, *82*, 93–99. [CrossRef]
31. Mulenshi, J.; Chelgani, S.C.; Rosenkranz, J. Mechanochemical Treatment of Historical Tungsten Tailings: Leaching While Grinding for Tungsten Extraction Using NaOH. *Sustainability* **2021**, *13*, 3258. [CrossRef]

Disclaimer/Publisher's Note: The statements, opinions and data contained in all publications are solely those of the individual author(s) and contributor(s) and not of MDPI and/or the editor(s). MDPI and/or the editor(s) disclaim responsibility for any injury to people or property resulting from any ideas, methods, instructions or products referred to in the content.